Efficient Blind Image Restoration Using Discrete Periodic Radon Transform

Daniel P. K. Lun, *Member, IEEE*, Tommy C. L. Chan, Tai-Chiu Hsung, *Member, IEEE*, David Dagan Feng, *Fellow, IEEE*, and Yuk-Hee Chan, *Member, IEEE*

***Abstract*—Restoring an image from its convolution with an unknown blur function is a well-known ill-posed problem in image processing. Many approaches have been proposed to solve the problem and they have shown to have good performance in identifying the blur function and restoring the original image. However, in actual implementation, various problems incurred due to the large data size and long computational time of these approaches are undesirable even with the current computing machines. In this paper, an efficient algorithm is proposed for blind image restoration based on the discrete periodic Radon transform (DPRT). With DPRT, the original two-dimensional blind image restoration problem is converted into one-dimensional ones, which greatly reduces the memory size and computational time required. Experimental results show that the resulting approach is faster in almost an order of magnitude as compared with the traditional approach, while the quality of the restored image is similar.**

***Index Terms*—ARMA processes, image deblurring, Radon transforms.**

I. Introduction

THE IMAGE-formation process can often be formulated by a linear model as [1]

$$g(x,y) = \sum_{x'=0}^{N-1}\sum_{y'=0}^{N-1} f(x-x', y-y')h(x',y') + n(x,y) \quad (1)$$

where N is the image size, $f(x,y)$ is the original image, $g(x,y)$ is the observed image, $h(x,y)$ is the point spread function (PSF), and $n(x,y)$ is the additive noise due to the imaging system. The problem of image restoration is to recover an unknown original image $f(x,y)$ from a given blurred image $g(x,y)$ and the PSF $h(x,y)$. Different approaches have been proposed [2]–[4] to solve this problem and they have shown to have good performance when prior information of the original image is acquired. Unfortunately, these approaches rely on the assumption that full information of the PSF is available can hardly be fulfilled in many practical situations. Without the prior information of the PSF, the restoration problem becomes the so-called blind image restoration, which can be tackled as a single problem or divided into two steps, that is, "blindly" identifying the PSF and then performing the image restoration. A good review on this topic can be found in [5].

Manuscript received February 27, 2001; revised May 21, 2003. This work was supported by the Hong Kong University Grant Council under Research Project Q134. The associate editor coordinating the review of this manuscript and approving it for publication was Dr. Ivan W. Selesnick.

The authors are with the Centre for Multimedia Signal Processing, Department of Electronic and Information Engineering, The Hong Kong Polytechnic University, Kowloon, Hong Kong (e-mail: enpklun@polyu.edu.hk).

Digital Object Identifier 10.1109/TIP.2004.823820

One of the important approaches for solving the blind restoration problem is based on the ARMA parameter estimation method as described in [5]. These approaches model the true image as a two-dimensional (2-D) autoregressive (AR) process and the PSF as a 2-D moving average (MA) process. Hence, the resulting blurred image can be represented as an autoregressive moving average (ARMA) process. Identifying the ARMA parameters allows us to identify the true image and PSF. The maximum-likelihood (ML) estimation [6] and generalized cross-validation (GCV) approaches [7] are the two most popular approaches to estimate the ARMA parameters. The ML approach has a long history for ARMA parameter estimation. It accomplishes the estimation by seeking for the parameters that are most likely to have produce the blurred image on hand. The GCV approach on the other hand achieves the estimation by looking for the parameters that minimize a weighted sum of prediction errors. This criterion has been shown to possess certain properties that are superior to those of ML in the regularization parameter estimation [8] and perform much better for real images [7], [9]. However, the GCV approach is often criticized due to extensive numerical searches for minimizing the GCV score. Efficient approach [10] was proposed to first estimate the unknown PSF parameter set and regularization parameter from raw data, and then make use of a computationally inexpensive algorithm to solve the nonblind problem. However, this approach requires multiple blurred versions (or low-resolution) of the original image during restoration (or super-resolution) that imposes limitation to general applications.

In this paper, we consider adopting the discrete periodic Radon transform (DPRT) [11] to estimate the PSF. The recently proposed DPRT has many properties similar to the conventional continuous Radon transform [12]. They include the discrete Fourier slice theorem and circular convolution property [11]. Using these properties, a 2-D signal can be processed by some one-dimensional (1-D) approaches to reduce the computational complexity. DPRT is different from other discrete Radon transform [13] in that it has an exact inverse transform. In this paper, we shall elaborate on how to convert the 2-D blind image restoration problem to the 1-D ones using DPRT. Experimental results show that the new approach can be an order of magnitude faster than the traditional approach, while the quality of the restored image is similar. The memory requirement is also dramatically reduced. Since the proposed approach is just a fast algorithm to the original 2-D GCV algorithm, it shares the same advantages and limitations in applications. For instance, the GCV methods are usually less

sensitive to additive noise than methods of other classes of blind deconvolution techniques because they take into account the noise in the system [5]. However, since the GCV methods deal only with the second-order signal statistics, phase cannot be identified uniquely in the restoration procedure. Hence, the GCV approaches are usually used for restoring images blurred by linear motion or the out-of-focus PSFs, which are symmetric and zero phase in nature.

II. DPRT

Denote the set of real number as $\mathbf{R}$, $\mathbf{R} \times \mathbf{R}$ as $\mathbf{R}^2$, the set of integers as $\mathbf{Z}$, $\mathbf{Z} \times \mathbf{Z}$ as $\mathbf{Z}^2$, a subset of integers $\{0, 1, 2, \ldots, n-1\} \in \mathbf{Z}$ as $\mathbf{Z}^n$, and $\mathbf{Z}^n \times \mathbf{Z}^n$ as $\mathbf{Z}_n^2$. Let $f(x, y)$ be a 2-D function with $x, y \in \mathbf{Z}$. The DPRT of $f(x, y)$ on $\mathbf{Z}_P^2$ or $\mathbf{Z}_{2^n}^2$, where P is a prime integer and n is any positive integer, were proposed in [11] as follows.

Case 1:

$$\{f(x,y): x, y \in \{0, 1, \ldots, P-1\}, \text{where } P \text{ is prime}\}.$$

The DPRT of $f(x, y)$ in this case is defined as the following set of formulations:

$$f_m^c(d) = \sum_{x=0}^{P-1} f(x, < d + mx >_P) \tag{2a}$$

$$f_0^b(d) = \sum_{y=0}^{P-1} f(d, y) \tag{2b}$$

where $\langle A \rangle_D$ refers to the residue of A modulo D; $d, m \in \{0, 1, \ldots, P-1\}$.

Case 2:

$$\{f(x,y): x, y \in \{0, 1, \ldots, N-1\}, \text{where } N = 2^n, n \in \mathbf{Z}\}.$$

The DPRT of $f(x, y)$ in this case is defined as the following set of formulations:

$$f_m^c(d) = \sum_{x=0}^{2^n-1} f(x, < d + mx >_{2^n}) \tag{3a}$$

$$f_s^b(d) = \sum_{y=0}^{2^{n-1}-1} f(< d + 2sy >_{2^n}, y) \tag{3b}$$

where $d, m \in \{0, 1, \ldots, 2^n - 1\}$; $s \in \{0, 1, \ldots, 2^{n-1} - 1\}$. Both $f_s^b(d)$ and $f_m^c(d)$ represent the summations of discretized contents in $f(x, y)$ with parameters $\{m, s\}$ and d. To draw an analogy with the conventional Radon transform, we may consider $f_m^c(d)$ and $f_s^b(d)$ as the projections of $f(x, y)$ in different angles "m" and "s" and different distances "d" from the origin. We shall use the term "projection" in the later part of this paper to indicate the DPRT of a function with a particular m or s. Fig. 1 shows the DPRT of a function f with support size 3×3.

DPRT has a few important properties, such as the discrete Fourier slice theorem and convolution property [11], which are particularly useful in image processing. With the convolution property, a 2-D circular convolution can be decomposed into

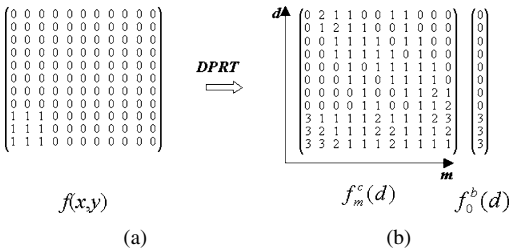

Fig. 1. Example of the prime-length DPRT. (a) Original 2-D function. (b) The DPRT of $f(x, y)$.

1-D circular convolutions. More specifically, if $g(x, y)$, $f(x, y)$, and $h(x, y)$ are all 2-D functions with supports $P \times P$, where P is a prime number, such that

$$g(x, y) = f(x, y) \otimes_2 h(x, y)$$

where $\otimes_2$ stands for 2-D cyclic convolution. It can be shown that, after DPRT

$$g_m^c(d) = h_m^c(d) \otimes f_m^c(d) \tag{4}$$

$$g_0^b(d) = h_0^b(d) \otimes f_0^b(d) \tag{5}$$

where $d, m \in \{0, \ldots, P-1\}$. The symbol $\otimes$ stands for 1-D circular convolution. The functions $\left(g_m^c(d), g_0^b(d)\right)$, $\left(h_m^c(d), h_0^b(d)\right)$, and $\left(f_m^c(d), f_0^b(d)\right)$ are the DPRT's of $g(x, y)$, $h(x, y)$, and $f(x, y)$, respectively. By performing the inverse DPRT on $g_m^c(d)$ and $g_0^b(d)$, the convolution result $g(x, y)$ can be obtained. The inversion of DPRT on $\mathbf{Z}_p^2$ is given by

$$f(x,y) = \frac{1}{P}\left[\sum_{m=0}^{P-1} f_m^c(< y - mx >_P) - \sum_{d=0}^{P-1} f_0^b(d) + f_0^b(x)\right]. \tag{6}$$

It is observed that, except for the scaling factor $1/P$, only additions are required to evaluate (6). Indeed, both the forward and inverse DPRT require only additions for their implementations. This is particularly useful to some computing environments where the complexity of implementing multiplications is much higher than additions. Details of properties and inversion of DPRT can be found in [11]. Nevertheless, DPRT also has some undesirable features that make it difficult to apply in some image processing applications. As shown in Fig. 1, the basic version of DPRT is not orthogonal (although an orthogonal version is deemed to be available [14]). Redundancy is introduced after the transformation; hence, DPRT is basically not suitable to image compression. Secondly, DPRT of a compact-supported function is not necessarily compact support, as is shown in Fig. 1. We shall show that this undesirable feature introduces much difficulty in blind image restoration problems.

III. GCV for Image Restoration

The GCV image restoration algorithm assumes that the image formation and blurring processes follow some specific models. It has been shown from (1) that the degraded image model can be

viewed as a 2-D MA process in the presence of noise. The image formation process can also be modeled as a 2-D AR process

$$f(p,q) = \sum_{(k,l)\in R_a} a_{kl} f(p-k, q-l) + u(p,q) \tag{7}$$

where $f(p,q)$ is the pixel value of the original image at (p,q), $u(p,q)$ is an independent zero-mean white noise with variance σ_u^2, and R_a is the nonsymmetric half-plane (NSHP) support [15] of the AR process, respectively. Equations (1) and (7) can be further represented in a compact form as

$$f = \bar{a} f + u \tag{8}$$

$$g = \bar{h} f + n \tag{9}$$

where the 2-D signals have been lexicographically ordered. h and a are expressed in matrix-vector notations as $\bar{h}$ and $\bar{a}$. Equations (8) and (9) can be combined to form a single equation

$$g = \bar{h}(I - \bar{a})^{-1} u + n. \tag{10}$$

The blur identification becomes a matter of determining the parameters of an ARMA model.

Cross validation is well recognized in data analysis. It is also known as "leave-one-out" [16] or predictive sample reuse [17]. Use of cross validation in image restoration is simple. For a fixed model parameter set, a restored image is determined using all but one of the values from the observed image. The restored image is then reblurred to predict the observation that was left out of the restoration. The process is iterated, using different set of parameters each time, until all values from the observed image have been exhausted. The parameter set that minimizes the mean-square prediction error over all the observations is chosen as the optimal estimate. Due to the difficulty in implementation, the cross-validation approach is modified [14] to become the generalized cross validation, which is a rotation invariant form of the ordinary cross validation. The parameter set minimizing the following GCV score is taken to be the final solution

$$V(\theta) = N^2 \frac{\sum_{i=0}^{N^2-1} \left[\frac{\alpha}{|\gamma_i(\theta)|^2+\alpha}\right]^2 |\hat{g}_i|^2}{\left[\sum_{i=0}^{N^2-1} \frac{\alpha}{|\gamma_i(\theta)|^2+\alpha}\right]^2} \tag{11}$$

where $\theta = \{\alpha, \bar{h}, \bar{a}\}$ is the parameter set to be estimated. $\bar{h}$ and $\bar{a}$ are the PSF and image model parameters, α is the regularization parameter, respectively. The functions $\gamma_i(\theta)$ and $\tilde{g}_i$ in (11) relates to $\bar{h}$ and $\bar{a}$ as follows. Let the singular value decomposition of $\bar{h}\,(I-\bar{a})^{-1}$ be $U\Gamma V^T$, then $\hat{g}_i$ are the elements of $U^T g$ and γ_i are the diagonal entries of Γ, where g is the observed image and T denotes the complex conjugate transpose operator. The expected value of the GCV criterion attains a global minimum at the true values of the ARMA model parameters [7]. In practice, due to the huge sizes of $\bar{h}$ and $\bar{a}$ (each has the size of $N^2 \times N^2$), (11) is often implemented in the frequency domain as shown in (12), at the bottom of the page, where H, A, and G are 2-D DFT of h, a, and g, respectively. $conj(H)$ and $conj(B)$ are the complex conjugate of H and B, with $B = I - A$. Here we have assumed that the matrices A and H are circulant. It implies that the image has been blurred by a circular convolution operation. This assumption has been used in many traditional image restoration algorithms [6], [7] to reduce the computational complexity. As long as the image boundaries are properly preprocessed to remove false boundary discontinuities, the circular convolution assumption has a negligible effect on the identification results. Besides, it is further assumed in many traditional approaches that most images can be represented adequately as a process whose autocorrelation function consists of a separable exponentially decaying sequence [6], [7]. It results in a much simplified AR model that can be described by only two parameters as follows: $a_{10} = \rho_v$, $a_{01} = \rho_h$, and $a_{11} = -\rho_v \rho_h$; where a_{ij} represents the AR formation model parameter for the original image. Moreover, the blurring process is assumed to be energy conservative, that is $\sum_{(k,l)\in R_h} h_{kl} = 1$; where R_h is the support of the blur function. The energy conservation assumption is valid due to the fact that a fixed number of photons are detected regardless of whether blurring occurs.

IV. Converting 2-D GCV to 1-D GCVs Using DPRT

The GCV criterion is clearly nonlinear in the parameters of interest and cannot be minimized analytically; therefore, numerical techniques are used to determine the parameter set. It has been shown [7] that the numerical search performs particularly well for single parameter PSF. However, in the case of blurring due to multiple-parameter PSF, it is often required to carry out numerical optimization procedure for more than a few hundred iterations before the procedure converges. It requires a long computation time since, for each iteration, the GCV score for a 2-D signal is to be determined. In addition, the huge volume of memory transfers due to the buffering of 2-D signals also requires a significant amount of computation time.

Since DPRT is able to convert a 2-D circular convolution problem into 1-D ones, it is intuitively to consider using DPRT for blind image restoration. The idea is very simple. Recall (8) and (9) and rewrite them using the circular convolution operator

$$f = \tilde{a} \otimes_2 f + u \tag{13}$$

$$g = \tilde{h} \otimes_2 f + n. \tag{14}$$

Since the support of the PSF and AR models is often much smaller than the image, the function $\tilde{h}$ and $\tilde{a}$ as shown in (13) and (14) refer to the original h and a padded with the appropriate

$$V(\theta) = \frac{\frac{1}{N^2}\sum_{p=0}^{N-1}\sum_{q=0}^{N-1}\left(1 - \frac{(conj(H)^* H)_{p,q}}{(conj(H)^* H)_{p,q} + \alpha (conj(B)^* B)_{p,q}}\right)^2 |G_{p,q}|^2}{\left[1 - \frac{1}{N^2}\sum_{p=0}^{N-1}\sum_{q=0}^{N-1}\frac{(H'H)_{p,q}}{(conj(H)^* H)_{p,q} + \alpha (conj(B)^* B)_{p,q}}\right]^2} \tag{12}$$

number of zeros to enable them to have the same size as the image support. Assume that the DPRT of g, f, $\tilde{h}$, $\tilde{a}$, u, and n are (g_m^c, g_s^b), (f_m^c, f_s^b), $(\tilde{h}_m^c, \tilde{h}_s^b)$, $(\tilde{a}_m^c, \tilde{a}_s^b)$, (u_m^c, u_s^b), and (n_m^c, n_s^b), respectively, where $m = 0, \ldots 2^{n-1} - 1$. $s = 0, \ldots, 2^{n-1} - 1$ and the size of all functions are $N \times N$, where $N = 2^n; n \in \mathbf{Z}$. Then, from the circular convolution property of DPRT, we have

$$\begin{aligned} f_m^c &= f_m^c \otimes \tilde{a}_m^c + u_m^c \quad g_m^c = f_m^c \otimes \tilde{h}_m^c + n_m^c \\ f_s^b &= f_s^b \otimes \tilde{a}_s^b + u_s^b \quad g_s^b = f_s^b \otimes \tilde{h}_s^b + n_s^b \end{aligned} \tag{15}$$

which shows that the original 2-D blind image restoration problem is converted into $3N/2$ 1-D blind image restoration problems. The 1-D GCV algorithm can be applied to estimate $\left(\tilde{h}_m^c, \tilde{h}_s^b\right)$, $(\tilde{a}_m^c, \tilde{a}_s^b)$ from $(\tilde{g}_m^c, \tilde{g}_s^b)$. The 1-D GCV score for the m projection becomes (16), as shown at the bottom of the page, where $\tilde{H}_m^c$ and G_m^c are the DFT of $\tilde{h}_m^c$ and g_m^c, respectively. $\tilde{B}_m^c$ is the DFT of b_m^c, with $\tilde{b}_m^c = I - \tilde{a}_m^c$. The parameter set θ_m in this case becomes $\{\alpha_m, \tilde{h}_m^c, \tilde{a}_s^b\}$. The 1-D GCV scores for the s projections are similar to (16) with all m replaced by s. Let us summarize the whole procedure as follows.

1) Transform the observed image g into the DPRT domain to become (g_m^c, g_s^b).
2) Apply 1-D GCV algorithm to estimate $(\tilde{h}_m^c, \tilde{h}_s^b)$ and $(\tilde{a}_m^c, \tilde{a}_s^b)$ from $(\tilde{g}_m^c, \tilde{g}_s^b)$.
3) Reconstruct $\tilde{h}$ and $\tilde{a}$ based on $(\tilde{h}_m^c, \tilde{h}_s^b)$, $(\tilde{a}_m^c, \tilde{a}_s^b)$ using the inverse DPRT [11].
4) Obtain the restored image using any computationally inexpensive restoration algorithm based on the estimated $\tilde{h}$ and $\tilde{a}$.

V. Proposed DPRT Blind Image Restoration Algorithm

Unfortunately, the intuitive idea suggested in Section IV does not work properly in general. Due to the nonorthogonal property of DPRT, the $3N/2$ 1-D GCV restorations have the total computational complexity not so much less than the original 2-D problem. Furthermore, as is mentioned above, the DPRT of a compact-supported function may not be compact supported. It implies that more parameters will be required to estimate than the original 2-D approach. Let us use an example to illustrate the problem. Assume that g has the size of 256×256. Assume also that h and a have the size of 5×5 and 2×2, respectively. Hence, originally the parameter set contains only 30 parameters are required to be estimated. In (15), the support for $(\tilde{h}_m^c, \tilde{h}_s^b)$, $(\tilde{a}_m^c, \tilde{a}_s^b)$ can be up to 256, i.e., the size of the image support. It implies that for each m and s, up to 256 parameters are required to be estimated. It is simply unachievable with the GCV algorithm. Consequently, it is known that direct blind image restoration using DPRT is not feasible. In this paper, we modify the algorithm such that only a few essentially compact-supported projections are used for the restoration. In this way, the computational complexity is greatly reduced.

It is interesting to note that, depending on the size of h and $\tilde{h}$, some of the projections of $\tilde{h}$ are compact supported. It is shown in the following lemma.

Lemma 1: Given that a function $\tilde{h}$ with size $N \times N$ is formed by padding appropriate number of zeros to another function h with size $P \times P$, where $N = 2^n; n \in \mathbf{Z}$ and P is a prime integer. If the DPRT of $\tilde{h}$ is $(\tilde{h}_m^c(d), \tilde{h}_s^b(d))$, where $m, d = 0, \ldots N-1$; $s = 0, \ldots, N/2 - 1$, then

$$\begin{aligned} \tilde{h}_m^c(d) = 0, \quad \text{if} \Big\{ & P \le d \le N - 1 \\ & - m(P-1) \text{ and } m < \frac{N-P}{P-1} \Big\} \\ \text{or if} \Big\{ & P + (N-m)(P-1) \le d \le \\ & N - 1 \text{ and } m > N - \frac{N-P}{P-1} \Big\} \\ \tilde{h}_s^b(d) = 0, \quad \text{if} \Big\{ & P \le d \le N - 1 - 2s(P-1) \\ & \text{and } s < \frac{N-P}{2(P-1)} \Big\} \\ \text{or if} \Big\{ & P + (N-2s)(P-1) \le d \le N-1 \\ & \text{and } s > \frac{N}{2} - \frac{N-P}{2(P-1)} \Big\}. \end{aligned} \tag{17}$$

The proof of Lemma 1 is shown in Appendix A. In fact, Lemma 1 only describes a special case that N is a power of 2 and P is a prime number. A more general lemma can be derived to deal with different combinations of N and P. However, the case for (17) is typical for many image restoration problems. Lemma 1 shows that when m and s are very small or very big numbers, there will be a consecutive sequence of zeros in the projection. This implies that the first and the last few projections of the total $3N/2$ projections are essentially compact supported. From (17), we can also derive the support size of some of the essentially compact-supported projections. For instance, if $S(\cdot)$ refers to the support size of a projection, we know that

$$\begin{aligned} S\left(\tilde{h}_m^c\right) &= P + m(P-1) \text{ for } m < \frac{N-1}{P-1} \\ S\left(\tilde{h}_m^c\right) &= P + (N-m)(P-1) \text{ for } m > N - \frac{N-1}{P-1} \\ S\left(\tilde{h}_s^c\right) &= P + 2s(P-1) \text{ for } s < \frac{N-1}{2(P-1)} \\ S\left(\tilde{h}_s^c\right) &= P + 2\left(\frac{N}{2} - s\right)(P-1) \text{ for } s > \frac{N}{2} - \frac{N-1}{2(P-1)}. \end{aligned} \tag{18}$$

$$V(\theta_m) = \frac{\frac{1}{N}\sum_{p=0}^{N-1}\left(1 - \frac{(conj(\tilde{H}_m^c)^* \tilde{H}_m^c)_p}{(conj(\tilde{H}_m^c)^* \tilde{H}_m^c)_p + \alpha_m (conj(\tilde{B}_m^c)^* \tilde{B}_m^c)_p}\right)^2 \left|G_m^c(p)\right|^2}{\left[1 - \frac{1}{N}\sum_{p=0}^{N-1} \frac{(conj(\tilde{H}_m^c)^* \tilde{H}_m^c)_p}{(conj(\tilde{H}_m^c)^* \tilde{H}_m^c)_p + \alpha_m (conj(\tilde{B}_m^c)^* \tilde{B}_m^c)_p}\right]^2} \tag{16}$$

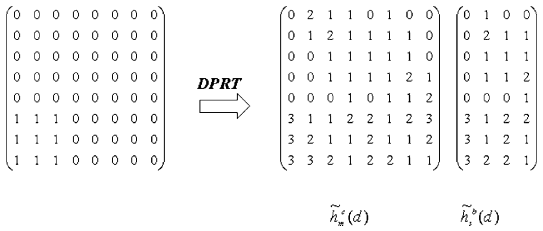

(a) (b)

Fig. 2. Example to illustrate Lemma 1. (a) Original 2-D function $\bar{h}$. (b) The DPRT of $\bar{h}$.

Fig. 2 provides an example to illustrate Lemma 1. In Fig. 2(a), a 3×3 2-D function h is padded with zeros to form an 8×8 function $\tilde{h}$. The DPRT of the zero-padded function is shown in Fig. 2(b). It is seen that the first few and last few columns (projection) of $\left(\tilde{h}_m^c(d),\tilde{h}_s^b(d)\right)$ are essentially compact supported.

In the previous example, it is shown that some of the projections are essentially compact supported. When applying the 1-D GCV algorithm to these essentially compact-supported projections, the number of parameters to be estimated is much less than the other projections. We now further show that only some of these essentially compact-supported projections are useful for reconstructing the original compact-supported PSF h. More specifically, we show in Lemma 2 that, if we acquire P essentially compact-supported projections from $\tilde{h}_m^c(d)$ and the first projection from $\tilde{h}_s^b(d)$, we can obtain (h_m^c,h_0^b) (i.e., the DPRT of h) by some simple additions on these projections. Consequently, we can reconstruct h from (h_m^c,h_0^b) based on the inverse DPRT as shown in (6).

Lemma 2: Given that a function $\tilde{h}$ with size $N\times N$ is formed by padding appropriate number of zeros to another function h with size $P\times P$, where $N=2^n; n\in\mathbf{Z}$ and P is a prime integer. Assume that the DPRT of $\tilde{h}$ is $\left(\tilde{h}_m^c(d),\tilde{h}_s^b(d)\right)$, where $m,\ d=0,\dots N-1;\ s=0,\dots,N/2-1$, and the DPRT of h is (h_m^c,h_0^b), where $m,\ d=0,\dots,P-1$. Assume also that $N>(P^2+1)$, then

$$\begin{aligned}
&\text{(i) } h_0^b(d)=\tilde{h}_0^b(d) \quad \text{for } d=0,\dots,P-1\\
&\text{(ii) } h_m^c(d)=\sum_{n=0}^{m-\lfloor m/P\rfloor}\tilde{h}_m^c(\langle d+P(N-n)\rangle_N) \quad \text{for}\\
&\qquad 0\le m<\frac{P}{2} \text{ and } d=0,\dots,P-1\\
&\text{(iii) } h_{P-1-m}^c(d)=\sum_{n=0}^{m-\lfloor m/P\rfloor}\tilde{h}_{N-1-m}^c(\langle d+Pn\rangle_N) \text{ for}\\
&\qquad 0\le m<\frac{P}{2} \text{ and } d=0,\dots,P-1. \qquad (19)
\end{aligned}$$

The proof of Lemma 2 is shown in Appendix B. Lemma 2 shows that by appropriately adding the data of the essentially compact-supported projections obtained from $\left(\tilde{h}_m^c(d),\tilde{h}_s^b(d)\right)$, we can reconstruct (h_m^c,h_0^b). More importantly, only $P+1$ projections are required for the reconstruction of (h_m^c,h_0^b) as compared to the original $3N/2$ projections. The computational complexity is greatly reduced.

Equation (19) allows us to evaluate (h_m^c,h_0^b) from $\left(\tilde{h}_m^c(d),\tilde{h}_s^b(d)\right)$ and then h can be obtained from (h_m^c,h_0^b) using the inverse DPRT. Besides estimating the PSF, the estimation of the image model parameters a is also important. The procedure for evaluating a can be much simplified due to the assumption we made. Recall that images are assumed to be represented adequately by an AR model a that can be described by only two parameters as follows: $a_{10}=\rho_v$, $a_{01}=\rho_h$, and $a_{11}=-\rho_v\rho_h$; where a_{ij} represents the parameter of the AR formation model for the original image. With this simple structure, all parameters can be easily obtained from the DPRT projections of $\tilde{a}$. More specifically, it is easy to show that

$$\tilde{a}_0^c(0)=\rho_v,\quad \tilde{a}_0^b(0)=\rho_h. \qquad (20)$$

Hence, once $\tilde{a}_0^c$ and $\tilde{a}_0^b$ are obtained from the 1-D GCV algorithm, ρ_v and ρ_h can also be obtained. When both h and a are available, the only thing missing is the regularization parameter α. It can be easily obtained by a direct search and using the 2-D GCV score as the stopping criterion.

Let us summarize the proposed DPRT blind image restoration algorithm as follows. Recall (13) and (14) for g and h with sizes equal to $N\times N$ and $P\times P$, respectively, where $N=2^n; n\in\mathbf{Z}$, and P is a prime integer. Then, with proper boundaries adjustment of g and f such that the circular convolutions in (13) and (14) are equivalent to the linear convolutions in (8) and (10), the proposed DPRT blind image restoration algorithm is as follows.

1) Perform DPRT on g to obtain (g_m^c,g_s^b) which are equal to the circular convolutions of (f_m^c,f_s^b) and $(\tilde{h}_m^c,\tilde{h}_s^b)$, respectively, as in (15).
2) Select g_0^b and P other projections from g_m^c of which the corresponding projections of $\tilde{h}_m^c$ are essentially compact supported. More specifically, we select the first $\lceil P/2\rceil$ and the last $\lfloor P/2\rfloor$ projections of g_m^c and projection g_0^b.
3) 1-D GCV algorithm is then applied to identify $(\tilde{h}_m^c,\tilde{h}_0^b)$ and $(\tilde{a}_m^c,\tilde{a}_0^b)$ for the selected projections.
4) Reconstruct (h_m^c,h_0^b) from $(\tilde{h}_m^c,\tilde{h}_0^b)$ using (19).
5) Obtain a from $(\tilde{a}_0^c,\tilde{a}_0^b)$ using (20).
6) Obtain h from (h_m^c,h_0^b) using the inverse DPRT algorithm as stated in (6).
7) Based on the estimated h and a, obtain α by direct searching and using the 2-D GCV score as the stopping criterion.
8) Restore the image using the estimated h, a, and α.

A block diagram is given in Fig. 3 to illustrate the procedure.

VI. Implementation Issues

As the other traditional approaches [6], [7], we only consider symmetric blur models in this paper. It is known that many real-life blurs—linear motion, out-of-focus, and atmospheric turbulence blurs—are symmetric. This assumption is not restrictive. More importantly, it greatly reduces the search space that allows the optimization procedure to converge more easily.

When the PSF is symmetric, we can easily show that its DPRT projections are also symmetric up to a rotation. Furthermore, some projections differ from the other only by a rotation. All these imply that the number of parameters to be estimated can

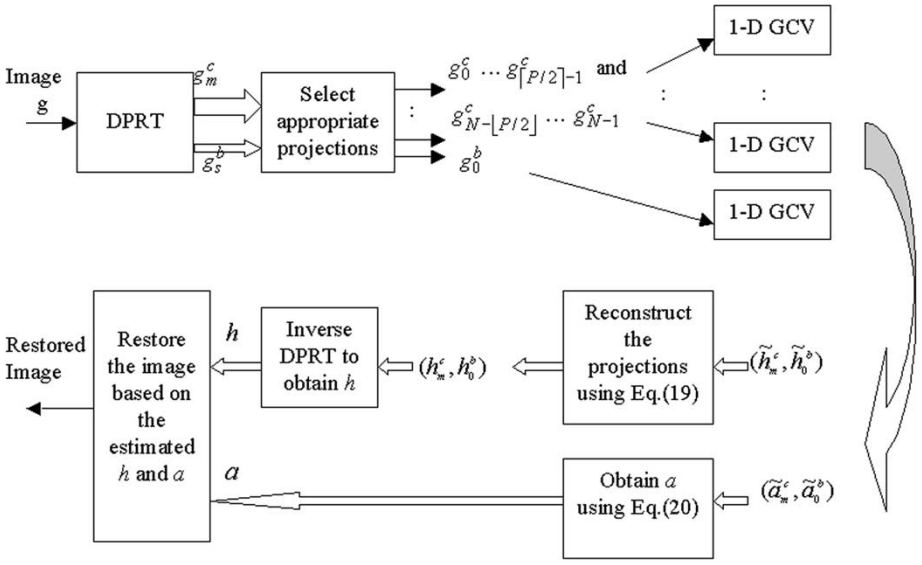

Fig. 3. Block diagram that describes the flow of the proposed algorithm.

be greatly reduced in the DPRT domain. Let us formally summarize these properties of DPRT as follows:

Lemma 3: Given that a function $\tilde{h}$ with size $N \times N$ is formed by padding appropriate number of zeros to another function h with size $P \times P$, where $N = 2^n; n \in \mathbf{Z}$ and P is a prime integer. Assume that the DPRT of $\tilde{h}$ is $\left(\tilde{h}^c_m(d), \tilde{h}^b_s(d)\right)$, where $m, d = 0, \ldots, N/2-1$; $s = 0, \ldots, N/2-1$, and the DPRT of h is (h^c_m, h^b_0), where $m, d = 0, \ldots P-1$. If h is symmetric such that

$$h(x,y) = h(< P-x-1 >_P, < P-y-1 >_P)$$

where $x, y = 0, \ldots, P-1$, then the following are true.

1) $\left(\tilde{h}^c_m(d), \tilde{h}^b_s(d)\right)$ is also symmetric up to a rotation.
2) $\tilde{h}^c_0(d) = \tilde{h}^b_0(d)$.
3) $abs\left(\mathrm{DFT}\left(\tilde{h}^c_m(d), \tilde{h}^b_s(d)\right)\right) = abs\big(\mathrm{DFT}\big(\tilde{h}^c_{N-m}(d), \tilde{h}^b_{N/2-s}(d)\big)\big)$, where $m = 1, \ldots N-1; s = 1, \ldots, N/2-1$.

The proof of Lemma 3 is shown in Appendix C. Item 1 of Lemma 3 implies that, for every projection in this case, only half of the coefficients are required to be estimated. The other half is the same as the first half. Item 2 of Lemma 3 implies that the coefficients of $\tilde{h}^c_0$ are the same as $\tilde{h}^b_0$. Hence, only one set of them needs to be estimated. Item 3 of Lemma 3 implies that for the P projections required to be estimated as indicated in Lemma 2, $(P-1)/2$ of them need not be estimated if h is symmetric. It is because they have the same coefficients as the other $(P-1)/2$ projections.

Let us use an example to further illustrate the actual numbers of coefficients need to be estimated for various projections. Let g have the size of 256×256 and h has the size of 5×5. Based on Lemma 2, we know that only g^c_0, g^c_1, g^c_2, g^c_{255}, g^c_{256} and g^b_0 are required in order to estimate h. From Lemma 3, we know that $\tilde{h}^c_0$ and $\tilde{h}^b_0$ have the same coefficients. Hence we only need to perform 1-D GCV algorithm on g^c_0 to obtain both $\tilde{h}^c_0$ and $\tilde{h}^b_0$. Furthermore, we know from Lemma 3 that $(\tilde{h}^c_1, \tilde{h}^c_2)$ and $(\tilde{h}^c_{255}, \tilde{h}^c_{256})$ have the same set of coefficients. Again, we only need to perform 1-D GCV algorithm on (g^c_1, g^c_2) to obtain both $(\tilde{h}^c_1, \tilde{h}^c_2)$ and $(\tilde{h}^c_{255}, \tilde{h}^c_{256})$. Finally, when estimating $(\tilde{h}^c_0, \tilde{h}^c_1, \tilde{h}^c_2)$ from the projections (g^c_0, g^c_1, g^c_2), Lemma 3 indicates that half of the coefficients of $(\tilde{h}^c_0, \tilde{h}^c_1, \tilde{h}^c_2)$ are the same as the other due to the symmetric property. For (18), we know that the support for $(\tilde{h}^c_0, \tilde{h}^c_1, \tilde{h}^c_2)$ are 5, 9, and 13, respectively. Due to the symmetry property, only 3, 5, and 7 of them, respectively, need to be estimated.

VII. Experimental Results

To verify the improvement achieved by the proposed approach, the traditional 2-D GCV blind image restoration algorithm and the proposed DPRT-based algorithm were implemented and compared. Both algorithms were implemented using Matlab and the command *fmincon* was used in both cases for numerical search. To improve the convergence rate of both approaches, a nonlinear constraint was imposed to the PSF during estimation. The nonlinear constraint is basically a band-reject filter to minimize the high frequency component of the PSF. We found that this constraint is particularly important to the 2-D GCV algorithm, as it was indicated in [19]. For both approaches, the following 5×5 PSF was used:

$$\begin{bmatrix} 0.0100 & 0.0248 & 0.0287 & 0.0248 & 0.0100 \\ 0.0248 & 0.0377 & 0.0812 & 0.0377 & 0.0248 \\ 0.0287 & 0.0812 & 0.1712 & 0.0812 & 0.0287 \\ 0.0248 & 0.0377 & 0.0812 & 0.0377 & 0.0248 \\ 0.0100 & 0.0248 & 0.0287 & 0.0248 & 0.0100 \end{bmatrix}.$$

The initial conditions for the 2-D GCV approach were

$$\Big\{\alpha = 0.0001; \rho_v = 0.8; \rho_h = 0.8; \quad h_{00} = 1; h_{ij} = 0; \text{ for } (i,j) \neq (0,0)\Big\}.$$

TABLE I
COMPARISON IN TERMS OF ARITHMETIC OPERATIONS REQUIRED

	2-D GCV			Proposed DPRT approach		
Noise Level (BSNR)	No. of iterations (I)	No of. Flops per iter. (F)	I×F	No. of iterations (I)	No of. flops per iter. (F)	I×F + DPRT
35dB	298	5,554,950	1.66×10^9	1,145	40,759	4.67×10^7
30dB	352	5,554,950	1.96×10^9	1,228	40,759	5.0×10^7

The initial conditions for the proposed DPRT-based algorithm were

$$\left\{\alpha_m = 0.0001; \rho_v = 0.8; \rho_h = 0.8 \right.$$
$$\left. \tilde{h}_m^c(0) = 1; \tilde{h}_m^c(d) = 0; \text{ for } d \neq 0 \right\}$$
$$\left\{\alpha_s = 0.0001; \rho_v = 0.8; \rho_h = 0.8 \right.$$
$$\left. \tilde{h}_0^b(0) = 1; \tilde{h}_0^b(d) = 0; \text{ for } d \neq 0 \right\}.$$

They were selected rather arbitrarily. Different standard testing images, such as Lenna and Pepper, were used and blurred by the PSFs. Additive white Gaussian noise was then added to the blurred image in two different noise levels, $\mathrm{BSNR} = 30$ dB and 40 dB, where BSNR is defined as

$$\mathrm{BSNR} = 10 \times \log_{10}\left(\frac{\text{blurred image power}}{\text{noise variance}}\right).$$

To simulate the restoration process for realistic photographically blurred images, we only extract the central 256×256 pixels of the noisy blurred images for restoration. The boundaries of the extracted images were preprocessed to remove the effects of boundary discontinuities. The approach we used is similar to [7] that for each extracted 256×256 pixels image, five pixels were removed on each side, and the boundary values were interpolated to smooth any discontinuities. For each image, 20 experiments were performed for each approach at two different noise levels ($\mathrm{BSNR} = 30$ dB and 35 dB). The results in terms of accuracy and complexity in all experiments were recorded and averaged. The accuracy was measured by the signal-to-error ratio between the restored image and the original image. The accuracy in estimating the PSF was also measured in terms of signal-to-error ratio. The complexity of the algorithms was measured by the required number of floating-point operations (flops) as reported by the *flops* command of Matlab. Since the major computation is in the numerical search, the number of flops in each iteration and the number of iterations for both approaches were recorded and compared. Table I shows a comparison of the computational complexity of the 2-D GCV algorithm and the proposed DPRT-based algorithm.

TABLE II
COMPARISON IN TERMS OF ACCURACY ACHIEVED

	2-D GCV		Proposed DPRT approach	
Noise level (BSNR)	Restored image accuracy (SER)	Estimated PSF accuracy (SER)	Restored image accuracy (SER)	Estimated PSF accuracy (SER)
35dB	29.44 dB	11.32 dB	30.89 dB	14.15 dB
30dB	28.92 dB	10.42 dB	29.31 dB	13.40 dB

Note that the result on "number of iterations" of the DPRT approach is the sum of all iterations required for the estimation of the parameter set in all projections. Note also that the floating-point operations required for the implementation of DPRT itself are also included and added to the results of the proposed DPRT-based approach. Table I shows that, in both noise levels, the total number of operations required for the proposed approach is only about 3% of the 2-D GCV algorithm. This result is foreseeable because the major operation done in each iteration of the GCV algorithm is an FFT. By converting a 2-D GCV algorithm to become some 1-D ones, the $N \times N$-point 2-D FFT required in each iteration is also converted into some N-point 1-D FFTs. For an image with size 256×256, a 256-point 1-D FFT requires only 0.2% of floating-point operations as compared with a 256×256-point 2-D FFT. So although a few more 1-D GCV algorithms need to be implemented in the proposed approach, the overall complexity is still only 3% of the 2-D case. Indeed the actual computation time required by the 2-D approach can be even longer than the proposed DPRT algorithm due to the massive 2-D data transfer, of which the burden introduced has not been reflected in the number of arithmetic operations reported. This kind of data movement is particularly slow in Matlab if it is not carefully handled. Table II illustrates the accuracy of both approaches.

(a) (b)

(c) (d)

Fig. 4. (a) Original Lena (256×256). (b) Blurred and noisy Lena ($\mathrm{BSNR} = 30$ dB). (c) Restored Lena using 2-D GCV ($\mathrm{SER} = 27.13$ dB). (d) Restored Lena using the proposed DPRT approach ($\mathrm{SER} = 27.86$ dB).

The results in Table II show that the accuracy of the proposed DPRT approach is comparable, if not better, than the traditional 2-D approach. Both approaches have the problem of jumping into local minimum during numerical search. The problem happened more often when noise level is lowered to $\mathrm{BSNR} = 35$ dB. For the proposed approach, this problem happens about five times in each 20 experiments. However, the problem can often be solved by restarting the algorithm with the estimated parameters serving as the initial guess plus a random turbulence. The result for model parameter estimation is not shown here since the estimation result varied from one experiment to another. This happens to both approaches since the image model is only an approximation to the actual one. Figs. 4 and 5 show the actual restored images given by both approaches. They can be considered as a subjective measure for the accuracy of the algorithms. However, it is seen that no observable difference can be found from the restored images obtained by the two approaches.

VIII. Conclusion

In this paper, efficient algorithms are proposed for blind image restoration. By using the discrete periodic Radon transform, the original 2-D blind image restoration problem is converted to some 1-D ones, and hence greatly reduces the memory size and computation time. Experimental results show that the proposed DPRT-based approach consistently uses less arithmetic operations than the 2-D GCV approach. Apart from the savings in computation time, the accuracy of the proposed approach is comparable, if not better, than the traditional one in both objective and subjective measures. While the proposed approach is only a fast algorithm to the original one, it shares the same limitations. For example, the GCV algorithm can only estimate the magnitude of the PSF but not the phase information. Besides, as with most of the traditional approaches, the support of the PSF is assumed to be known in the proposed algorithm. This assumption may not be valid in some practical

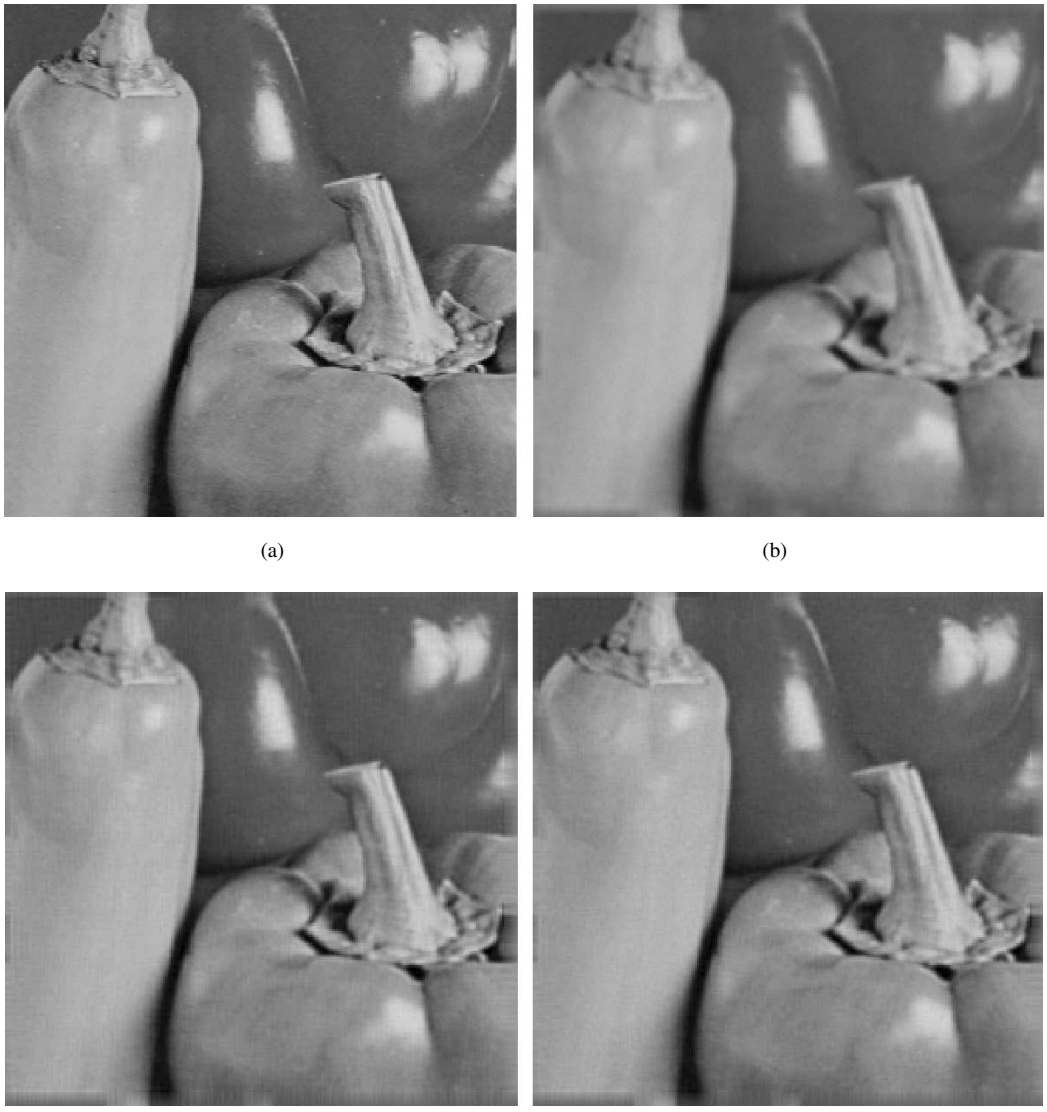

(a) (b)

(c) (d)

Fig. 5. (a) Original pepper (256×256). (b) Blurred and noisy pepper ($\mathrm{BSNR} = 30$ dB). (c) Restored Pepper using 2-D GCV ($\mathrm{SER} = 30.72$ dB). (d) Restored pepper using the proposed DPRT approach ($\mathrm{SER} = 30.77$ dB).

situations. It means that a prior process may be required to estimate the support of the PSF. Some results from the work on ARMA model order estimation [20] can be used to deal with this problem. Further work is being carried out to tackle these two problems.

APPENDIX I

Proof of Lemma 1

Given that a function $\tilde{h}$ with size $N \times N$ is formed by padding appropriate number of zeros to another function h with size $P \times P$, where $N = 2^n; n \in \mathbf{Z}$ and P is a prime integer. Given also that the DPRT of $\tilde{h}$ is $(\tilde{h}^c_m(d), \tilde{h}^b_0(d))$ such that

$$\tilde{h}^c_m(d) = \sum_{x=0}^{N-1} \tilde{h}(x, < d + mx >_N) \tag{A.1}$$

$$\tilde{h}^b_s(d) = \sum_{y=0}^{N-1} \tilde{h}(< d + 2sy >_N, y) \tag{A.2}$$

where $m, d = 0, \ldots, N-1; s = 0, \ldots, N/2 - 1$. From (A.1), we know that

$$\begin{aligned}\tilde{h}^c_m(d) &= \sum_{x=0}^{N-1} \tilde{h}(x, < d + mx >_N) \\ &= \sum_{x=0}^{P-1} \tilde{h}(x, < d + mx >_N) \\ &\quad + \sum_{x=P}^{N-1} \tilde{h}(x, < d + mx >_N).\end{aligned}$$

Since

$$\tilde{h}(x,y)=0 \text{ if } x,y>P-1.$$

Hence, if

$$\sum_{x=0}^{P-1}\tilde{h}(x,\langle d+mx\rangle_N)=0 \quad \Rightarrow \quad \tilde{h}_m^c(d)=0.$$

Or equivalently, if $\langle d+mx\rangle_N \geq P \;\forall\; x \leq P-1 \quad \Rightarrow \tilde{h}_m^c(d)=0$.

Let us consider for all m such that $m(P-1)<N-P$. Hence, $N-1-m(P-1)\geq P$. Consider for all d such that $P\leq d\leq N-1-m(P-1)$. Since $0\leq x\leq P-1$

$$P\leq d+mx\leq N-1, \text{ if } P\leq d\leq N-1-m(P-1). \quad \text{(A.3)}$$

That is

$$\begin{aligned}\langle d+mx\rangle_N &= d+mx\geq P \text{ if}\\ &P\leq d\leq N-1-m(P-1) \text{ and}\\ &m<\frac{N-P}{P-1}.\end{aligned}$$

Hence, $\tilde{h}_m^c=0$ if $P\leq d\leq N-1-m(P-1)$ and $m<(N-P/P-1)$ Q.E.D.

Let us consider for all m such that $m>N-(N-P/P-1)$. Hence, $P+(N-m)(P-1)\leq N-1$. Consider for all d such that $P+(N-m)(P-1)\leq d\leq N-1$

$$\begin{aligned}&P+(N-m)(P-1)+mx\leq d+mx \text{ if}\\ &P+(N-m)(P-1)\leq d\leq N-1.\end{aligned}$$

Let $k=N-m$

$$\begin{aligned}&P+k(P-1)+(N-k)x\leq d+(N-k)x \text{ if}\\ &P+k(P-1)\leq d\leq N-1.\end{aligned}$$

Since $x\leq P-1$

$$\begin{aligned}&P+Nx\leq d+(N-k)x, \text{ if}\\ &P+k(P-1)\leq d\leq N-1.\end{aligned}$$

Hence

$$\begin{aligned}&P\leq d+mx-Nx \text{ if}\\ &P+(N-m)(P-1)\leq d\leq N-1.\end{aligned}$$

Since $0\leq x$ and $d\leq N-1$

$$d+mx-Nx=d-(N-m)x\leq N-1.$$

Hence

$$\begin{aligned}P\leq d+mx-Nx\leq N-1, \text{ if}\\ P+(N-m)(P-1)\leq d\leq N-1 \text{ and}\\ m>N-\frac{N-P}{P-1}.\end{aligned}$$

That is

$$\begin{aligned}\langle d+mx\rangle_N\geq P, \text{ if}\\ P+(N-m)(P-1)\leq d\leq N-1 \text{ and}\\ m>N-\frac{N-P}{P-1}.\end{aligned}$$

Hence, $\tilde{h}_m^c=0$ if $P+(N-m)(P-1)\leq d\leq N-1$ and $m>N-N-P/P-1$ Q.E.D.

The proof for $\tilde{h}_s^b$ is similar to that described above.

APPENDIX II

Proof of Lemma 2

Given that a function $\tilde{h}$ with size $N\times N$ is formed by padding appropriate number of zeros to another function h with size $P\times P$, where $N=2^n; n\in \mathbf{Z}$ and P is a prime integer. It is known that $N>P^2+1$, and the DPRT of $\tilde{h}$ is $(\tilde{h}_m^c(d),\tilde{h}_s^b(d))$ such that

$$\tilde{h}_m^c(d)=\sum_{x=0}^{N-1}\tilde{h}(x,\langle d+mx\rangle_N) \quad \text{(B.1)}$$

$$\tilde{h}_s^b(d)=\sum_{y=0}^{N-1}\tilde{h}(\langle d+2sy\rangle_N,y) \quad \text{(B.2)}$$

where $m, d=0,\ldots,N-1; s=0,\ldots,N/2-1$. The DPRT of h is $(\tilde{h}_m^c(d),h_0^b(d))$ such that

$$h_m^c(d)=\sum_{x=0}^{P-1}h(x,\langle d+mx\rangle_P) \quad \text{(B.3)}$$

$$h_0^b(d)=\sum_{y=0}^{P-1}h(d,y) \quad \text{(B.4)}$$

where $m, d=0,\ldots,P-1$. Since

$$\tilde{h}(x,y)=0 \text{ if } x,y>P-1 \quad \text{(B.5)}$$

we immediately have the following result:

$$h_0^b(d)=\tilde{h}_0^b(d) \text{ for } d=0,\ldots,P-1.$$

Hence, Lemma 2 case (i) is proved. (Q.E.D.)

The relationship between f_m^c and f_m^c can be proven as follows.

Since

$$\begin{aligned}\tilde{h}_m^c(d)&=\sum_{x=0}^{N-1}\tilde{h}(x,\langle d+mx\rangle_N)\\ &=\sum_{x=0}^{P-1}\tilde{h}(x,\langle d+mx\rangle_N)\\ &\quad+\sum_{x=P}^{N-1}\tilde{h}(x,\langle d+mx\rangle_N)\end{aligned}$$

from (B.5), we know that the second term is equal to 0. Hence

$$\tilde{h}_m^c(d)=\sum_{x=0}^{P-1}\tilde{h}(x,\langle d+mx\rangle_N). \quad \text{(B.6)}$$

For $m = 0, \ldots, (P-1)/2$

$$\begin{aligned}&\sum_{n=0}^{m-\lfloor m/P \rfloor} \tilde{h}_m^c(\langle d+(N-n)P\rangle_N)\\ &= \sum_{n=0}^{m-\lfloor m/P \rfloor}\sum_{x=0}^{P-1} \tilde{h}(x, \langle d+mx-nP\rangle_N)\\ &= \sum_{x=0}^{P-1}\sum_{n=0}^{m-\lfloor m/P \rfloor} \tilde{h}(x, \langle d+mx-nP\rangle_N). \end{aligned} \quad \text{(B.7)}$$

(B.7) shows that if

$$\sum_{n=0}^{m-\lfloor m/P \rfloor} \tilde{h}(x, \langle d+mx-nP\rangle_N) = h(x, \langle d+mx\rangle_P) \quad \text{(B.8)}$$

then the proof of Lemma 2 case (ii) is completed. Indeed, the maximum value of the term $d+mx$ can also be determined to be

$$d+mx \le \frac{P-1+((P-1)^2)}{2} \le \frac{(P^2-1)}{2} < N.$$

Hence, since both d, x and m are positive integers, the term $h(x, < d+mx >_p)$ can be rewritten as follows:

$$h(x, \langle d+mx\rangle_P) = h(x, \langle d+mx-iP\rangle_N) \quad \text{(B.9)}$$

for an integer i. From the maximum values of d and x, we can determine the maximum value of i for different m as follows:

$$i \le m - \left\lfloor \frac{m}{P} \right\rfloor \quad \text{(B.10)}$$

and

$$iP \le m(P-1) + \langle m\rangle_P < N \quad \text{(B.11)}$$

since $N > (P^2+1)$. Consequently, given that $\tilde{h}(x,y) = 0$ for $x, y > P-1$ as specified in (B.5), we have

$$\tilde{h}(x, \langle d+mx-nP\rangle_N) = \begin{cases} h(x, \langle d+m-iP\rangle_N) & \text{if } n = i \\ 0, & \text{if } n \ne i \end{cases}$$

for $n = 0, \ldots, m - \lfloor m/P \rfloor$. Thus, we have

$$\begin{aligned}&\sum_{n=0}^{m-\lfloor m/P \rfloor} \tilde{h}(x, \langle d+mx-nP\rangle_N)\\ &= h(x, d+mx-iP)\\ &= h(x, \langle d+mx\rangle_P).\end{aligned}$$

Lemma 2 case (ii) is thus proven. (Q.E.D.)

Lemma 2 case (iii) can be proven similarly. We need to prove that

$$\begin{aligned}&\sum_{n=0}^{m-\lfloor m/P \rfloor} \tilde{h}(x, \langle d+(N-1-m)x+nP\rangle_N)\\ &= h(x, \langle d+(P-1-m)x\rangle_P)\end{aligned}$$

for $d, x = 0, \ldots, P-1; m = 0, \ldots, (P-1)/2$. The maximum value of the term $d+(P-1-m)x$ can be determined to be

$$\begin{aligned}&d+(P-1-m)x \le P-1\\ &+(P-1)(P-1) \le (P^2-P) < N.\end{aligned}$$

Hence, since both d, x and m are all positive integers, the term $h(x, < d+(P-1-m)x >_P)$ can be rewritten as follows:

$$\begin{aligned}&h(x, < d+(P-1-m)x >_P)\\ &= h(x, < d+Px-x-mx-iP >_N)\\ &= h(x, < d+(N-1-m)x+(x-i)P >_N)\\ &= h(x, < d+(N-1-m)x+i'P >_N)\end{aligned} \quad \text{(B.12)}$$

for an integer i. From the minimum value of d and the maximum value of x, we can determine the maximum value of i' for different m as follows:

$$i' \le m - \left\lfloor \frac{m}{P} \right\rfloor \quad \text{(B.13)}$$

and

$$i'P \le m(P-1) + \langle m\rangle_P < N \quad \text{(B.14)}$$

since $N > (P^2+1)$. Consequently, given that $\tilde{h}(x,y) = 0$ for $x, y > P-1$ as specified in (B.5), we have

$$\tilde{h}(x, < d+(N-1-m)x+nP >_N) = \begin{cases} h(x, < d+(N-1-m)x+iP >_N), & \text{if } n = i \\ 0, & \text{if } n \ne i \end{cases}$$

for $n = 0, \ldots, m - \lfloor m/P \rfloor$. Thus, we have

$$\begin{aligned}&\sum_{n=0}^{m-\lfloor m/P \rfloor} \tilde{h}(x, \langle d+(N-1-m)x+nP\rangle_N)\\ &= h(x, d+(N-1-m)x+iP)\\ &= h(x, \langle d+(N-1-m)x\rangle_P)\end{aligned}$$

for $d, x = 0, \ldots, P-1; m = 0, \ldots, (P-1)/2$. Lemma 2 case (iii) is thus proven. (Q.E.D.)

APPENDIX III

Proof of Lemma 3

Given that a function $\tilde{h}$ with size $N \times N$ is formed by padding the appropriate number of zeros to another function h with size $P \times P$, where $N = 2^n; n \in \mathbf{Z}$ and P is a prime integer. Both $\tilde{h}$ and h are assumed to be real functions. Assume also that the DPRT of $\tilde{h}$ is $\left(\tilde{h}_m^c(d), \tilde{h}_s^b(d)\right)$, where $m, d = 0, \ldots, N-1$; $s = 0, \ldots, N/2-1$, and the DPRT of h is (h_m^c, h_0^b), where m, $d = 0, \ldots, P-1$. Let the DFT of $\tilde{h}$ be $\tilde{H}$ and the DFT of h be H. Furthermore, let the DFT of $(\tilde{h}_m^c, \tilde{h}_s^b)$ be $(\tilde{H}_m^c, \tilde{H}_s^b)$. It is given that h is symmetric such that $h(x,y) = h(\langle P-x-1\rangle_P, \langle P-y-1\rangle_P)$.

(1) If h is symmetric and real, $\tilde{h}$ is also symmetric and real. Hence, $\tilde{H}$ will be symmetric in a sense that

$$\tilde{H}(u,v) = \tilde{H}^*(\langle N-u\rangle_N, \langle N-v\rangle_N)$$

where $u, v = 0, 1, \ldots, N-1$. where $\tilde{H}^*$ is the complex conjugate of $\tilde{H}$. Consider the discrete Fourier slice theorem [11] as

$$\begin{aligned}\tilde{H}_s^b(u) &= \tilde{H}(u, \langle -2su\rangle_N)\\ &= \sum_{d=0}^{N-1} \tilde{h}_s^b(d) \exp\left(\frac{-j2\pi ud}{N}\right)\end{aligned} \quad \text{(C.1)}$$

$$\tilde{H}_m^c(v) = \tilde{H}(\langle -mv\rangle_N, v) = \sum_{d=0}^{N-1} \tilde{h}_m^c(d) \exp\left(\frac{-j2\pi vd}{N}\right) \quad \text{(C.2)}$$

where $m = 0, 1, \ldots, N-1$; $s = 0, \ldots, N/2-1$. Since $\tilde{H}(u,v) = \tilde{H}^*(\langle N-u\rangle_N, \langle N-v\rangle_N)$, it implies that

$$\tilde{H}(u, \langle -2su\rangle_N) = \tilde{H}^*(\langle N-u\rangle_N, \langle N-(-2su)\rangle_N) = \tilde{H}^*(\langle N-u\rangle_N, \langle -2s(N-u)\rangle_N) \quad \text{(C.3)}$$

$$\tilde{H}(\langle -mv\rangle_N, v) = \tilde{H}(\langle N-(-mv)\rangle_N, \langle N-v\rangle_N) = \tilde{H}(\langle -m(N-v)\rangle_N, \langle N-v\rangle_N). \quad \text{(C.4)}$$

Equations (C.3) and (C.4) show that the DFTs of $\left(\tilde{h}_m^c(d), \tilde{h}_s^b(d)\right)$ are also symmetric. Hence, $\left(\tilde{h}_m^c(d), \tilde{h}_s^b(d)\right)$ must also be symmetric. However, since the imaginary part of $\left(\tilde{H}_m^c(d), \tilde{H}_s^b(d)\right)$ may not be equal to zero, $\left(\tilde{H}_m^c(d), \tilde{H}_s^b(d)\right)$ is only symmetric up to a rotation. (Q.E.D.)

(2) We know that

$$\tilde{h}_0^c(d) = \sum_{x=0}^{N-1} \tilde{h}(x,d) = \begin{cases} \sum_{x=0}^{P-1} h(x,d), & \text{for} \quad d = 0, \ldots, P-1 \\ 0, & \text{for} \quad N > d > P-1 \end{cases} \quad \text{(C.5)}$$

$$\tilde{h}_0^b(d) = \sum_{y=0}^{N-1} \tilde{h}(d,y) = \begin{cases} \sum_{y=0}^{P-1} h(d,y) & \text{for} \quad d = 0, \ldots, P-1 \\ 0 & \text{for} \quad N > d > P-1. \end{cases} \quad \text{(C.6)}$$

If h is symmetric, $h(x,y) = h(y,x)$. Hence

$$\sum_{x=0}^{P-1} h(x,d) = \sum_{y=0}^{P-1} h(d,y).$$

This implies that $\tilde{h}_0^c(d) = \tilde{h}_0^b(d)$. (Q.E.D.)

(3) If h is real and symmetric such that $h(x,y) = h(\langle P-x-1\rangle_P, \langle P-y-1\rangle_P)$, $\tilde{H}$ will also be symmetric in the sense that

$$abs(\tilde{H}(u,v)) = abs(\tilde{H}(\langle N-u\rangle_N, v)) \quad \text{(C.7)}$$

$$abs(\tilde{H}(u,v)) = abs(\tilde{H}(u, \langle N-v\rangle_N)). \quad \text{(C.8)}$$

If the discrete Fourier slice theorem is considered

$$\tilde{H}_s^b(u) = \tilde{H}(u, \langle -2su\rangle_N) = \sum_{d=0}^{N-1} \tilde{h}_s^b(d) \exp\left(\frac{-j2\pi ud}{N}\right) \quad \text{(C.9)}$$

$$\tilde{H}_m^c(v) = \tilde{H}(\langle -mv\rangle_N, v) = \sum_{d=0}^{N-1} \tilde{h}_m^c(d) \exp\left(\frac{-j2\pi vd}{N}\right) \quad \text{(C.10)}$$

where $m = 0, 1, \ldots, N-1$; $s = 0, 1, \ldots, N/2-1$. Equations (C.7) and (C.8) imply that

$$abs(\tilde{H}(u, \langle -2su\rangle_N)) = abs(\tilde{H}(u, \langle N-(-2su)\rangle_N)) = abs(\tilde{H}(u, \langle -2\left(\frac{N}{2}-s\right)u\rangle_N)) \quad \text{(C.11)}$$

$$abs(\tilde{H}(\langle -mv\rangle_N, v)) = abs(\tilde{H}(\langle N-(-mv)\rangle_N, v)) = abs(\tilde{H}(\langle -(N-m)v\rangle_N, v)). \quad \text{(C.12)}$$

Equations (C.11) and (C.12) show that

$$abs\left(\mathrm{DFT}\left(\tilde{h}_m^c(d), \tilde{h}_s^b(d)\right)\right) = abs\left(\mathrm{DFT}\left(\tilde{h}_{N-m}^c(d), \tilde{h}_{N/2-s}^b(d)\right)\right)$$

where $m = 1, \ldots, N-1$; $s = 1, \ldots, N/2-1$.

This implies the coefficients of projections (m,s) and $(N-m, N/2-s)$ are identical up to a rotation. (Q.E.D.)

REFERENCES

[1] H. C. Andrews and B. R. Hunt, *Digital Image Restoration*. Englewood Cliffs, NJ: Prentice-Hall, 1977.

[2] N. P. Galatsanos and A. K. Katsaggelos, "Methods for choosing the regularization parameter and estimating the noise variance in image restoration and their relation," *IEEE Trans. Image Processing*, vol. 1, pp. 322–336, July 1992.

[3] A. K. Katsaggelos, "Iterative image restoration algorithm," *Opt. Eng.*, vol. 28, no. 7, pp. 735–748, July 1989.

[4] R. W. Schafer, R. M. Mersereau, and M. A. Richards, "Constrained iterative restoration algorithms," *Proc. IEEE*, vol. 69, pp. 432–450, Apr. 1981.

[5] D. Kundur and D. Hatzinakos, "Blind image deconvolution," *IEEE Signal Processing Mag.*, pp. 43–64, May 1996.

[6] R. L. Lagendijk, J. Biemond, and D. E. Boekee, "Identification and restoration of noisy blurred images using the expectation-maximization algorithm," *IEEE Trans. Acoust., Speech, Signal Processing*, vol. 38, pp. 1180–1191, July 1990.

[7] S. J. Reeves and R. M. Mersereau, "Blur identification by the method of generalized cross-validation," *IEEE Trans. Image Processing*, pp. 301–311, 1992.

[8] G. Wahba, "A comparison of GCV and GML for choosing the smoothing parameter in the generalized spline smoothing problem," *Annals Stat.*, vol. 13, no. 4, pp. 1378–1402, 1985.

[9] N. Fortier, G. Demoment, and Y. Goussard, "Implementation and practical comparison of two estimators of the smoothing parameter in linear image restoration," in *Proc. ICASSP'90*, 1990, pp. 1905–1908.

[10] N. Nguyen, G. Golub, and P. Milanfar, "Blind restoration/superresolution with generalized cross-validation using gauss-type quadrature rules," in *Proc. 33rd Asilomar Conf. Signals, Systems, and Computers*, vol. 2, 1999, pp. 1257–1261.

[11] T. C. Hsung, D. P. K. Lun, and W. C. Siu, "The discrete periodic radon transform," *IEEE Trans. Signal Processing*, vol. 44, pp. 2651–2657, Oct. 1996.

[12] S. R. Deans, *The Radon Transforms and Some of its Applications*. New York: Wiley, 1983.

[13] G. Beylkin, "Discrete radon transform," *IEEE Trans. Acoust., Speech, Signal Processing*, vol. 35, pp. 162–172, Feb. 1987.

[14] D. P. K. Lun and W. C. Siu, "An efficient in-place computation for the two-dimensional discrete fourier and hartley transform," in *Proc. ISCAS'92*, 1992, pp. 160–163.

[15] D. E. Dudgeon and R. M. Mersereau, *Multidimensional Digital Signal Processing*. Englewood Cliffs, NJ: Prentice-Hall, 1984.

[16] P. A. Devijver and J. Kittler, *Pattern Recognition: A Statistical Approach*. Englewood Cliffs, NJ: Prentice-Hall, 1982.

[17] S. Geisser, "The predictive sample reuse method with applications," *J. Amer. Statist. Assoc.*, vol. 27, no. 350, pp. 320–328, 1975.

[18] G. H. Golub, M. Heath, and G. Wahba, "Generalized cross-validation as a method for choosing a good ridge parameter," *Technometrics*, vol. 21, no. 2, pp. 215–223, May 1979.

[19] R. Whatmough, "Applying generalized cross-validation to image restoration," in *Proc. ICASSP'94*, vol. 5, 1994, pp. 453–456.
[20] X. D. Zhang and Y. S. Zhang, "Determination of the MA order of an ARMA process using sample correlations," *IEEE Trans. Signal Processing*, vol. 41, pp. 2657–2664, Aug. 1993.

Daniel P. K. Lun (M'91) received the B.Sc. (Hons.) degree from the University of Essex, Essex, U.K., and the Ph.D. degree from the Hong Kong Polytechnic University (formerly Hong Kong Polytechnic), Kowloon, Hong Kong, in 1988 and 1991, respectively.

He is currently an Associate Professor and the Associate Head of the Department of Electronic and Information Engineering of the Hong Kong Polytechnic University. His research interests include digital signal processing, wavelets, multimedia technology, and internet technology.

Dr. Lun was the Secretary, Treasurer, Vice-Chairman, and Chairman of the IEEE Hong Kong Chapter of Signal Processing in 1994, 1995–1996, 1997–1998, and 1999–2000, respectively. He was the Finance Chair of 2003 IEEE International Conference on Acoustics, Speech, and Signal Processing held in Hong Kong in April 2003. He is a Chartered Engineer and a Corporate Member of the Institution of Electronics Engineers (IEE).

Tommy C. L. Chan received the B.Eng. (Hons.) degree in 1998 from the Hong Kong Polytechnic University, Kowloon, Hong Kong, where he is currently working toward the Ph.D. degree.

His research interests include digital image processing and error-resilient image/video communications.

Tai-Chiu Hsung (M'93) received the B.Eng. (Hons.) and Ph.D. degrees in electronic and information engineering in 1993 and 1998, respectively, from the Hong Kong Polytechnic University, Kowloon, Hong Kong.

In 1999, he joined the Hong Kong Polytechnic University as a Research Fellow. His research interests include wavelet theory and applications, tomography, and fast algorithms.

Dr. Hsung is also a Member of the Institution of Electronics Engineers (IEE).

David Dagan Feng (F'02) received the Ph.D. degree in computer science from the University of California at Los Angeles (UCLA) in 1988.

After briefly working as Assistant Professor in U.S., he joined the University of Sydney, Sydney, Australia, as a Lecturer, Senior Lecturer, Reader, and then Professor. He is the former Head of Department of Computer Science/School of Information Technologies. He is currently Associate Dean of the Faculty of Science and Director of the Biomedical and Multmedia Information (BMIT) Research Group at the University of Sydney. He is also Professor and Deputy Director at the Center for Multimedia Signal Processing, Department of Electronic and Information Engineering, Hong Kong Polytechnic University. He has published over 300 scholarly research papers, pioneered several new research directions, and has made a number of landmark contributions in his field. Many of his research results have been translated into solutions to real-life problems worldwide and have made tremendous improvements to the quality of life.

Dr. Feng is currently Special Area Editor of the IEEE TRANSACTIONS ON INFORMATION TECHNOLOGY IN BIOMEDICINE, Advisor for the *International Journal of Image and Graphics*, Chairman of IFAC-TC-BIOMED, and Chairman of the International Programme and National Organizing Committees for the IFAC 2003 Symposium. He received the Crump Prize for Excellence in Medical Engineering. He is a Fellow of ACS, HKIE, and the Institution of Electronics Engineers (IEE).

Yuk-Hee Chan (M'92) received the B.Sc. degree (Hons.) in electronics from the Chinese University of Hong Kong in 1987, and the Ph.D. degree in signal processing from the Hong Kong Polytechnic University, Kowloon, Hong Kong, in 1992.

He joined the Hong Kong Polytechnic University in 1992 and is now an Associate Professor in the Department of Electronic and Information Engineering. He has published over 85 research papers in various international journals and conferences. His research interests include image and video compression, image restoration, and fast computational algorithms in digital signal processing.